



# Lamellar orientation in isotactic polypropylene thin films: a complement study via grazing incidence X-ray diffraction and surface/cross-sectional imaging

Kiminori Uchida <sup>1</sup> · Kazuki Mita <sup>1</sup> · Yuji Higaki <sup>2,3,4,5</sup> · Ken Kojio <sup>2,3,4</sup> · Atsushi Takahara <sup>2,3,4</sup>

Received: 20 July 2018 / Revised: 19 September 2018 / Accepted: 20 September 2018 / Published online: 29 October 2018  
© The Society of Polymer Science, Japan 2018

## Abstract

The crystalline structures of isotactic polypropylene (iPP) thin films were investigated using grazing incident wide-angle X-ray diffraction (GIWAXD), atomic force microscopy (AFM), and transmission electron microscopy (TEM). The out-of-plane (110) reflection split with 99° inclination in the GIWAXD pattern. The film surface was covered with flat-on mother lamellae with orthogonal daughter lamellae. The cross-sectional TEM image and the fast Fourier transform-processed image showed vertically aligned daughter lamellae and cross-hatched lateral mother lamellae. Flat-on lamellae may be preferentially produced at the substrate interface, after which the mother lamellae may yield daughter lamellae from the *ac* plane to give vertically aligned lamellae. The daughter lamellae yield in-plane lamellae with flat-on alignment from the *ac* plane, resulting in the global growth of a cross-hatched lamellar structure.

## Introduction

While isotactic polypropylene (iPP) is the most commonly used plastic material, crystal structure management has the potential to further expand its applications. Four polymorphs of crystalline iPP are known: the monoclinic  $\alpha$ -form (i.e., the dominant population), the pseudo-hexagonal  $\beta$ -form, the orthorhombic  $\gamma$ -form, and smectic forms [1–5]. The  $\alpha$ -form of iPP has a unique cross-hatched lamellar structure in which the daughter lamellae grow epitaxially on the *ac* plane of the mother lamellae [6, 7]. The *a* and *c* axes of the mother lamellae are parallel to the *c* and *a* axes of the daughter lamellae, respectively [8]. The  $\beta$  monoclinic angle is approximately 99° [9, 10].

Crystallization in polymer thin films on solid substrates has been researched because of its importance in industry. The crystallinity, melting temperature, lattice constants, and nucleation rate in thin films are totally different from those in the bulk [11–15]. The lamellae crystallites exhibit preferential orientation in thin films because of their confinement and interactions with the substrate. In edge-on lamellae, the chain axis (*c*-axis) is parallel to the substrate, while in flat-on lamellae, the chain axis is normal to the substrate [16]. The arrangement of crystals in thin films is significantly associated with the mechanical and optical properties of the films. The orientation of lamellae in crystalline polymer thin films can be determined using various techniques, including optical microscopy (OM) [17], atomic force microscopy (AFM) [18, 19], electron diffraction (ED) [19], reflection high-energy electron diffraction (RHEED) [20], grazing incidence reflection absorption Fourier transform infrared (RA-FTIR) spectroscopy [21], near-edge X-ray absorption fine structure

**Electronic supplementary material** The online version of this article (<https://doi.org/10.1038/s41428-018-0138-3>) contains supplementary material, which is available to authorized users.

✉ Kiminori Uchida  
Kiminori.Uchida@mitsuichemicals.com

<sup>1</sup> Process Technology Laboratory, Mitsui Chemicals Inc., 580-32 Nagaura, Sodegaura, Chiba 299-0265, Japan

<sup>2</sup> Institute for Materials Chemistry and Engineering, Kyushu University, Fukuoka, Japan

<sup>3</sup> Graduate School of Engineering, Kyushu University,

Fukuoka, Japan

<sup>4</sup> International Institute for Carbon-Neutral Energy Research (WPI-I2CNER), Kyushu University, 744 Motooka, Nishi-ku, Fukuoka 819-0395, Japan

<sup>5</sup> Present address: Department of Integrated Science and Technology, Faculty of Science and Technology, Oita University, 700 Dannoharu, Oita 870-1192, Japan

(NEXAFS) spectroscopy [22], grazing incident wide-angle X-ray diffraction (GIWAXD), and grazing incident small-angle X-ray scattering (GISAXS) [23, 24].

The lamellar orientation is sensitive to various factors. Flat-on lamellae gain precedence over edge-on lamellae as the film thickness decreases [25–27]. Flat-on lamellae are preferentially formed at high crystallization temperatures [28–30]. The interaction between polymer chains and the substrate plays an important part in the crystal orientation. The edge-on to flat-on transition has been observed in polyethylene thin films on silicon wafers as the film thickness decreases, while only edge-on lamellae were observed on aluminum films and a polyimide sheet [22]. Wang et al. [29] proposed a three-layered glass transition temperature ( $T_g$ ) model to rationalize the isothermal crystallization temperature dependence in lamellar orientation. In the surface region, polymer chain mobility is activated, leading to a reduction in  $T_g$ , whereas the substrate restricts the thermal molecular motion of the polymer chains, resulting in an increase in  $T_g$ . Because the primary nucleation rate depends on the chain mobility and chain/substrate interaction, the crystallization temperature is associated with the preferred location of nucleation. Yang et al. [31] calculated the critical free energies for flat-on and edge-on nucleation in terms of the local surface energy matching concept. The preferential edge-on or flat-on orientation of lamellar crystallites was predicted from the surface energies of the folding plane of the lamellae, the lateral plane of the lamellae, the polymer melt, and the substrates.

In iPP thin films, mother and daughter lamellae may grow in-plane at the same time, or one may grow in-plane and the other may grow out-of-plane. Although the lamellar orientation in crystalline polymer thin films has been investigated in a variety of polymer families, the lamellar orientation in orthogonal cross-hatched mother/daughter lamellar crystals in iPP thin films remains poorly understood. The molecular aggregation structure of iPP thin films has been investigated using AFM [32, 33] and ED [34, 35]; however, since AFM provides only local surface topographic data and ED provides average structural information in the thickness direction of thin films, the cross-hatched lamellar structure in thin films has not yet been examined in depth.

In this study, the lamellar orientation in iPP thin films on silicon wafer substrates was investigated using polarizing optical microscopy (POM), AFM, and GIWAXD. Transmission electron microscopy (TEM) imaging of the film's cross-section was also performed to provide complementary information on the mechanism of out-of-plane lamellar growth.

## Experimental procedures

Silicon (111) wafer substrates were modified with octyltrimethoxysilane (OTMS, Gelest) by the chemical vapor

adsorption method [36] to suppress the dewetting of the polymer films during isothermal crystallization. The silicon wafers were photochemically cleaned by exposure to an ultraviolet excimer lamp (UER20-172VB, Ushio Inc.) at a wavelength of 172 nm at 50 Pa for 10 min. The substrates were placed in a polytetrafluoroethylene container with a glass microtube containing 100  $\mu\text{L}$  of toluene and 12.5  $\mu\text{L}$  of silane coupling agents. The container was sealed with a cap under nitrogen and placed inside a stainless steel container, which was heated in an oven at 120  $^\circ\text{C}$  for 2 h. The substrates were then removed from the container and sequentially rinsed with toluene and ethanol. The contact angles of water and diiodomethane droplets on the substrate were measured, and the surface free energy (26.7  $\text{mJ m}^{-2}$ ) was calculated by the Owens–Wendt method [37].

The iPP (Cat. No. 06536-100) was purchased from Polysciences, Inc. (Warrington, PA, USA). Weight-average molecular weights ( $M_w$ ) and molecular weight distributions ( $M_w/M_n$ ) were determined by gel permeation chromatography (GPC) using a HLC-8321 GPC/HT (TOSOH) equipped with a refractive index detector. Polystyrene gel columns of TSKgel GMH6-HT and TSKgel GMH6-HTL (TOSOH) were connected, and measurements were performed at 140  $^\circ\text{C}$  using *o*-dichlorobenzene as the eluent at a flow rate of 1.0  $\text{mL min}^{-1}$ . A 20 mg sample of iPP was dissolved in 20 mL of *o*-dichlorobenzene by stirring at 145  $^\circ\text{C}$ . After filtration through a 1.0  $\mu\text{m}$  sintered metal filter, the solution was injected into the GPC system. The  $M_w$  and  $M_w/M_n$  were 386,000 and 7.5, respectively. The isotacticity was determined to be 91.9% by  $^{13}\text{C}$  nuclear magnetic resonance spectroscopy with *o*-dichlorobenzene/benzene- $d_6$  (4/1 vol./vol.) mixed solvent. Tetramethylsilane was used as the internal standard. The melting temperature was determined by differential scanning calorimetry (DSC) to be 162  $^\circ\text{C}$ . The DSC measurements were performed in the temperature range of  $-60$  to 200  $^\circ\text{C}$  at a scanning rate of 10  $^\circ\text{C} \cdot \text{min}^{-1}$  under dry nitrogen gas. The iPP thin films were prepared on silicon wafer substrates modified with OTMS from a 1.0 wt% *p*-xylene solution via the dip-coating method. The substrates were dipped into the polymer solution, after which the solution was heated to 140  $^\circ\text{C}$  for 5 min. The substrates were drawn up at a rate of 15  $\text{mm s}^{-1}$ . The as-cast films were dried in a nitrogen-filled box for 1 h; then, the thickness was determined by AFM observation of the scratch track. The thin films were melted at 172  $^\circ\text{C}$  for 10 min and then isothermally crystallized at 142  $^\circ\text{C}$  under nitrogen for 24 h.

GIWAXD measurements were performed at the BL03XU beamline of SPring-8 [38, 39]. The wavelength of the X-ray beam was 0.10 nm, and the camera length was 168 mm. The camera length was calibrated using a cerium oxide standard. The samples were mounted in a homemade

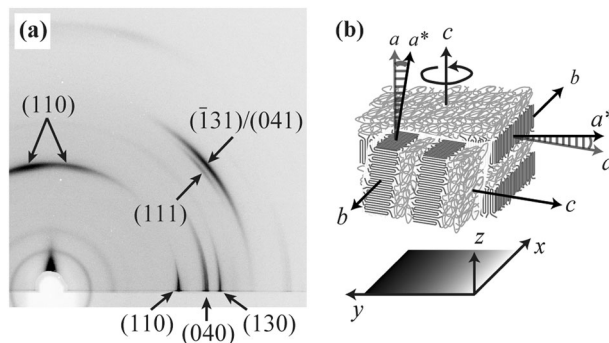
vacuum cell made of polyimide (KAPTON) thin film (15  $\mu\text{m}$  thickness) to avoid sample oxidation and scattering from air. The incident angles ( $\alpha_i$ ) of the X-ray to the film surface were  $0.08^\circ$  and  $0.16^\circ$ , which was smaller and larger than the critical angle ( $\alpha_c$ ) of the iPP ( $0.10^\circ$ ). GIWAXD patterns were acquired using a charge-integration type detector (SOPHIAS, RIKEN, Japan) with a detector plane of  $26.40\text{ mm} \times 63.0\text{ mm}$  and a pixel resolution of  $30\ \mu\text{m} \times 30\ \mu\text{m}$  [40]. Three images were acquired by changing the detector location; these were then merged. The exposure time was 3 s.

The morphology of the iPP thin film was observed by POM and AFM. POM images were taken using an ECLIPSE LV100 microscope (Nikon) in the reflection mode with crossed polarizers, and AFM was performed with a Cypher ES (Oxford Instruments) in the intermittent mode using aluminum-coated silicon cantilevers with a typical spring constant of  $26\text{ N m}^{-1}$  (OMCL-AC160TS-R3, OLYMPUS). Cross-sections of the iPP thin films on the silicon wafer substrate were prepared by milling the substrate using a focused ion beam (FIB) [41] followed by coating with carbon by thermal evaporation. The specimen was stained with  $\text{RuO}_4$  and then observed using a JEM-2200FS TEM (JEOL) with an accelerating voltage of 200 kV.

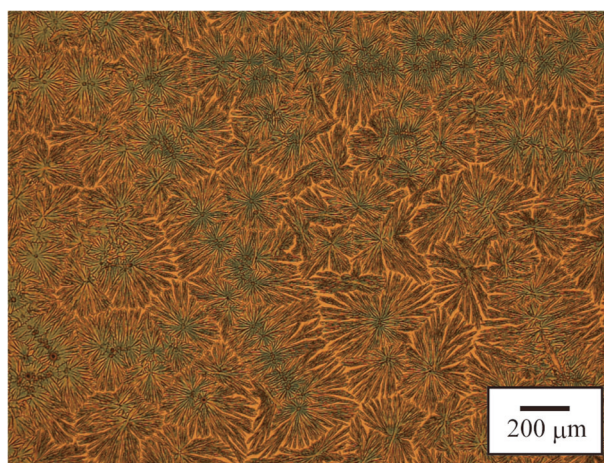
## Results and discussion

Figure 1a shows a typical two-dimensional GIWAXD pattern for the iPP thin film on a silicon wafer substrate measured at  $\alpha_i = 0.08^\circ$ . The penetration depth of the X-ray from the film surface depends on the  $\alpha_c$ . The penetration depth is limited to a single nanometer scale by setting the incident angle smaller than the critical angle. The (110), (040), (130), (111), and  $(\bar{1}31)/(041)$  reflections of monoclinic  $\alpha$ -form iPP crystals were clearly observed. All (hk0) reflections exhibit azimuthal broadening, and the intensity of the reflections reached their maximum at the in-plane. This result suggests that the  $c$ -axis of the monoclinic  $\alpha$ -form exhibited preferential alignment normal to the substrate, indicating that flat-on lamellae were produced in the thin films. In addition, the (110) reflection split at the out-of-plane, indicating lamellar branching. The  $c$ -axis of the  $\alpha$ -form unit cell in the daughter lamellae exhibited  $99^\circ$  inclination from the mother lamellae. Figure 1b illustrates the local lamellar orientation in the iPP thin film surface.

The surface morphology of the iPP thin films was determined by microscopic observations. During isothermal crystallization, the spherulites grew to a few hundred microns in diameter, as shown in the POM image (Fig. 2).



**Fig. 1** **a** GIWAXD pattern of the iPP thin films on an OTMS-modified silicon wafer substrate. The X-ray incident angle was  $0.08^\circ$ . **b** Schematic illustration of the preferential lamellar orientation in the iPP thin films

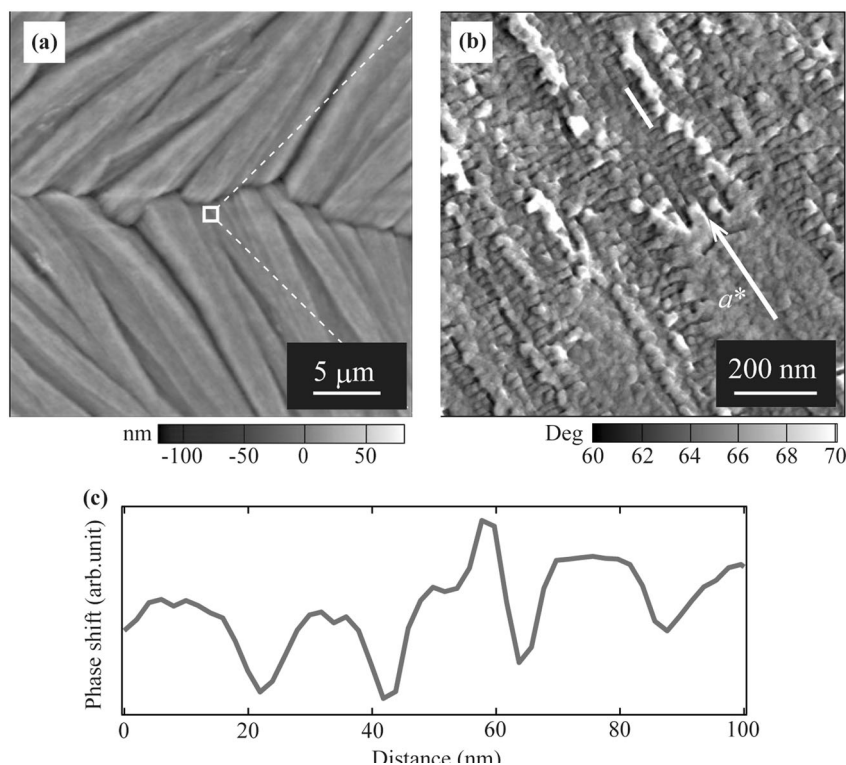


**Fig. 2** POM image of the iPP thin films after isothermal crystallization at  $142^\circ\text{C}$  under nitrogen for 24 h. Scale bar is  $200\ \mu\text{m}$

Figure 3a shows an intermittent mode AFM topographic image of the iPP spherulites. The fine structure was clearly observed in the phase contrast images (Fig. 3b). The growth direction of the iPP lamellae corresponded to the  $a^*$ -axis in a monoclinic unit cell [42, 43]. The arrow in Fig. 3b indicates the  $a^*$ -axis of the radial (mother) lamellae. A profusion of small tangential (daughter) lamellae were observed, as shown in Fig. 3b, in good agreement with the GIWAXD measurement results. Figure 3c shows a cross-sectional profile of the white solid line in Fig. 3b. The repetition period corresponded to the long period of the daughter lamellae, and the length was approximately 20 nm.

GIWAXD measurements and microscopic observations both revealed that cross-hatched lamellae with flat-on mother lamellae and orthogonal daughter lamellae were produced at the iPP film surface. The critical free energy difference between the flat-on primary nucleus,  $\Delta G_F^*$ , and the edge-on primary nucleus,  $\Delta G_E^*$ , can be expressed by the

**Fig. 3** Surface morphology of the iPP thin films after isothermal crystallization at 142 °C under nitrogen for 24 h. **a** AFM topographic image and **b** phase contrast image acquired in the intermittent mode. The white arrow indicates the  $a^*$ -axis direction of the mother lamellae. **c** A cross-sectional profile is shown of the white solid line in (b)



following equation: [31]

$$\Delta G_F^* - \Delta G_E^* = \frac{32(\sigma_{eC}^{1/2} - \sigma_C^{1/2})(\sigma_{eC}^{1/2} - \sigma_M^{1/2})(\sigma_C^{1/2} - \sigma_M^{1/2})^3(\sigma_S^{1/2} - \sigma_M^{1/2})}{\Delta f^2}, \quad (1)$$

where  $\sigma_{eC}$ ,  $\sigma_C$ ,  $\sigma_M$  and  $\sigma_S$  are the surface free energies of the folding plane of the crystal, lateral plane, melt, and substrate, respectively, and  $\Delta f$  is the free energy change upon crystallization per unit volume. The folding surface energy,  $\sigma_{eC}$  is much larger than the surface free energies of the lateral plane,  $\sigma_C$  and the melt,  $\sigma_M$ . The lateral surface energy,  $\sigma_C$  is reported to be  $11.5 \text{ mJ m}^{-2}$  [44]. The surface free energy of the polypropylene melt depends on temperature  $T$ ; it can be estimated by the following equation: [45]

$$\sigma_M = 29.4 - 0.056(T - 20), \quad (2)$$

where  $\sigma_M$  is estimated to be  $22.6 \text{ mJ m}^{-2}$  at 142 °C. When the surface energy of the substrate,  $\sigma_S$  ( $26.7 \text{ mJ m}^{-2}$ ), is substituted into Eq. 1,  $\Delta G_F^* - \Delta G_E^*$  becomes negative, indicating that flat-on primary nuclei are preferentially formed on the substrate. Meanwhile, because polymer chains tend to orient their longest dimension parallel to the surface [46], edge-on primary nuclei are intrinsically formed at the surface. The present results demonstrate that flat-on lamellae were yielded predominantly at the surface, indicating that nucleation and growth of lamellae occurred at the polymer–substrate

interface. The flat-on lamellae at the substrate interface grow in-plane, and the crystallization rate along the out-of-plane is much slower than that along the in-plane. Flat-on lamellae are preferred in ultrathin films, which are several tens of nanometers in thickness [25–27, 30, 47]. However, edge-on lamellae begin to predominate as the film thickness increases because the delayed nucleation at the surface is no longer negligible due to the slow out-of-plane growth rate of flat-on lamellae at the substrate interface.

Subsequently, the cross-sectional structure in the thin films was observed by means of TEM. Figure 4a shows the cross-sectional TEM image of the iPP thin films. The white arrow in Fig. 4a designates the carbon protective top layer for FIB milling. A periodic cylindrical structure with a lateral period of  $\sim 20 \text{ nm}$  was observed in the direction normal to the substrate. The long period was identical to that of the cross-sectional profile in the AFM phase image. In addition, the periodic structure was slightly observed in the direction parallel to the substrate. Figure 4b shows a fast Fourier transform-processed version of the image in Fig. 4a. The lateral periodic structure was inclined by approximately  $99^\circ$  with respect to the spot from the vertically aligned daughter lamellae, indicating that the lateral structure is the mother lamellae. Therefore, the cross-hatched structure consists of flat-on mother lamellae and edge-on daughter lamellar with vertical alignment. These periodic structures continuously appeared from the substrate interface to the thin film surface. The GIWAXD pattern measured at  $\alpha_i = 0.16^\circ$  (Figure S1) was identical to that measured at  $\alpha_i = 0.08^\circ$ . This result is consistent with the cross-sectional TEM image.

**Fig. 4** **a** Cross-sectional TEM image of the iPP thin films. The white arrow indicates the carbon protective layer. **b** Fast Fourier transform-processed image of the white frame area in (a). Two crystalline structures exhibited in cross-hatched form and inclined at approximately  $99^\circ$

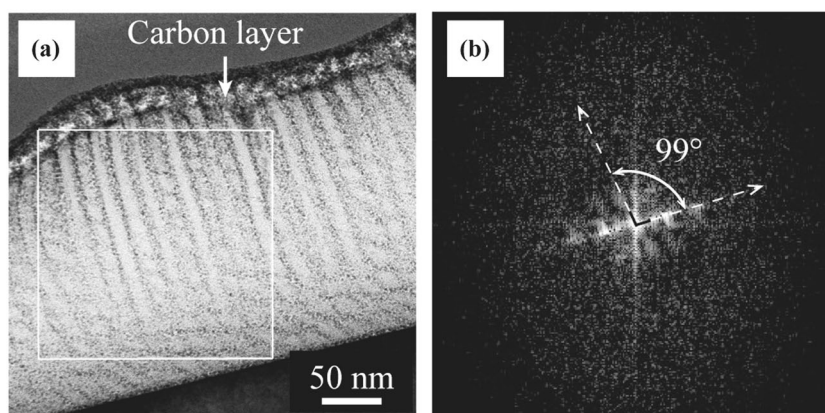
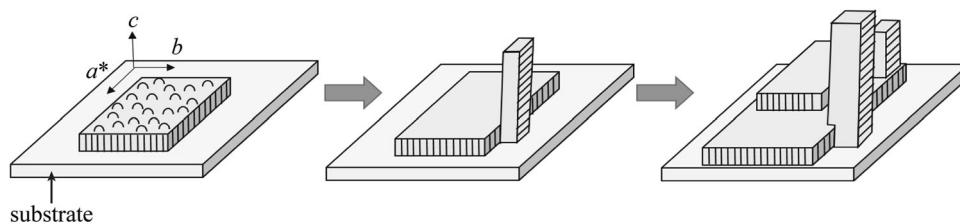


**Fig. 5** Schematic illustration of the crystallization process in the iPP thin films



The vertical daughter lamellae were fuzzy at the substrate interface, suggesting that the flat-on lamellae occupy the substrate interface because of the preceding nucleation and growth at the interface. The orthogonal daughter lamellae subsequently grew from the flat-on mother lamellae to produce vertically aligned lamellae with edge-on orientation.

Figure 5 provides a schematic illustration of the crystallization process in the iPP thin films proposed on the basis of the GIWAXD and TEM results.

(I) The flat-on lamellae nucleate on the substrate. The  $a^*$ -axis is parallel to the substrate. The flat-on lamellae anisotropically grow in-plane along the  $a^*$ -axis via repeating chain folding [35].

(II) The daughter lamellae are produced spontaneously from the  $ac$  plane of the flat-on mother lamellae. The epitaxial growth from the  $ac$  plane is induced by the matching of methyl group positions in the lattice [48]. When the  $c$ -axis (or  $a$ -axis) is parallel to the  $a$ -axis (or  $c$ -axis) of the mother lamellae, the methyl groups are located at the cavity between the methyl groups in the mother lamellae.

(III) The daughter lamellae subsequently grow from the mother lamellae at the substrate interface toward the film surface. The daughter lamellae yield in-plane lamellae with flat-on alignment from the  $ac$  plane, resulting in global growth of a cross-hatched lamellar structure.

## Conclusion

The crystalline structure in  $\alpha$ -iPP thin films was investigated by GIWAXD measurements and microscopic observations.

We propose a lamellar growth model for the iPP thin films in which the crystallization progresses from flat-on mother lamellar at the substrate interface to out-of-plane growth of the daughter lamellar from the mother lamellae. The flat-on mother lamellae preferentially form at the substrate interface, after which the daughter lamellae are epitaxially produced from the  $ac$  plane of the mother lamellae to give lamellae with edge-on alignment. The daughter lamellae show inclination of  $99^\circ$  to the substrate plane and yield in-plane lamellae with flat-on alignment to produce a global cross-hatched lamellar structure. Comprehensive insight into the ordered nucleation and growth in iPP will be important for further control of the crystalline structures of iPP film products.

**Acknowledgements** This work was partially supported by the Photon and Quantum Basic Research Coordinated Development Program of MEXT. The GIWAXD measurements were carried out at the first hutch of SPring-8 BL03XU constructed by the Consortium of Advanced Softmaterial Beamline (FSBL) (Proposal Nos. 2013A7218, 2013B7266, 2015A7216, 2015B7267, 2016A7217, and 2017B7267).

## Compliance with ethical standards

**Conflict of interest** The authors declare that they have no conflict of interest.

## References

1. Lotz B, Wittmann JC. The molecular origin of lamellar branching in the  $\alpha$  (monoclinic) form of isotactic polypropylene. *J Polym Sci Part B Polym Phys*. 1986;24:1541–58.

2. Brückner S, Meille SV, Petraccone V, Pirozzi B. Polymorphism in isotactic polypropylene. *Progress Polym Sci.* 1991;16:361–404.
3. Meille SV, Brückner S, Porzio W.  $\gamma$ -Isotactic polypropylene. A structure with nonparallel chain axes. *Macromolecules.* 1990;23:4114–21.
4. Mileva D, Androsch R, Zhuravlev E, Schick C. Temperature of melting of the mesophase of isotactic polypropylene. *Macromolecules.* 2009;42:7275–8.
5. Stocker W, Schumacher M, Graff S, Thierry A, Wittmann J-C, Lotz B. Epitaxial crystallization and AFM investigation of a frustrated polymer structure: isotactic poly(propylene),  $\beta$  phase. *Macromolecules.* 1998;31:807–14.
6. Padden FJ, Keith HD. Mechanism for lamellar branching in isotactic polypropylene. *J Appl Phys.* 1973;44:1217–23.
7. Yamada K, Matsumoto S, Tagashira K, Hikosaka M. Isotacticity dependence of spherulitic morphology of isotactic polypropylene. *Polymer.* 1998;39:5327–33.
8. Lotz B, Wittmann JC, Lovinger AJ. Structure and morphology of poly(propylenes): a molecular analysis. *Polymer.* 1996;37:4979–92.
9. Natta G, Corradini P. Structure and properties of isotactic polypropylene. *Il Nuovo Cim (1955–1965).* 1960;15:40–51.
10. Matick Z. Crystal structure of isotactic polypropylene. *J Macromol Sci Part B Phys.* 1972;6:101–15.
11. Frank CW, Rao V, Despotopoulou MM, Pease RFW, Hinsberg WD, Miller RD, et al. Structure in thin and ultrathin spin-cast polymer films. *Science.* 1996;273:912–5.
12. Nishino T, Matsumoto T, Nakamae K. Surface structure of isotactic polypropylene by X-ray diffraction. *Polym Eng Sci.* 2000;40:336–43.
13. Cho K, Kim D, Yoon S. Effect of substrate surface energy on transcrystalline growth and its effect on interfacial adhesion of semicrystalline polymers. *Macromolecules.* 2003;36:7652–60.
14. Yakabe H, Sasaki S, Sakata O, Takahara A, Kajiyama T. Paracrystalline lattice distortion in the near-surface region of melt-crystallized polyethylene films evaluated by synchrotron-sourced grazing-incidence X-ray diffraction. *Macromolecules.* 2003;36:5905–7.
15. Sakai A, Tanaka K, Fujii Y, Nagamura T, Kajiyama T. Structure and thermal molecular motion at surface of semi-crystalline isotactic polypropylene films. *Polymer.* 2005;46:429–37.
16. Liu Y-X, Chen E-Q. Polymer crystallization of ultrathin films on solid substrates. *Coord Chem Rev.* 2010;254:1011–37.
17. Grozev N, Botiz I, Reiter G. Morphological instabilities of polymer crystals. *Eur Phys J E Soft Matter.* 2008;27:63–71.
18. Kikkawa Y, Abe H, Fujita M, Iwata T, Inoue Y, Doi Y. Crystal growth in poly(L-lactide) thin film revealed by in situ atomic force microscopy. *Macromol Chem Phys.* 2003;204:1822–31.
19. Mareau VH, Prud'homme RE. In-situ hot stage atomic force microscopy study of poly( $\epsilon$ -caprolactone) crystal growth in ultrathin Films. *Macromolecules.* 2005;38:398–408.
20. Takenaka Y, Miyaji H, Hoshino A, Tracz A, Jeszka JK, Kucinska I. Interface structure of epitaxial polyethylene crystal grown on HOPG and MoS<sub>2</sub> substrates. *Macromolecules.* 2004;37:9667–9.
21. Liang Y, Zheng M, Park KH, Lee HS. Thickness-dependent crystal orientation in poly(trimethylene 2,6-naphthalate) films studied with GIWAXD and RA-FTIR methods. *Polymer.* 2008;49:1961–7.
22. Wang Y, Rafailovich M, Sokolov J, Gersappe D, Araki T, Zou Y, et al. Substrate effect on the melting temperature of thin polyethylene films. *Phys Rev Lett.* 2006;96:028303.
23. Asada M, Jiang N, Sendogdular L, Gin P, Wang Y, Endoh MK, et al. Heterogeneous lamellar structures near the polymer/substrate interface. *Macromolecules.* 2012;45:7098–106.
24. Sasaki S, Masunaga H, Tajiri H, Inoue K, Okuda H, Noma H, et al. In situ investigation of annealing effect on lamellar stacking structure of polyethylene thin films by synchrotron grazing-incidence small-angle and wide-angle X-ray scattering. *J Appl Crystallogr.* 2007;40(s1):s642–4.
25. Wang Y, Ge S, Rafailovich M, Sokolov J, Zou Y, Ade H, et al. Crystallization in the thin and ultrathin films of poly(ethylene–vinyl acetate) and linear low-density polyethylene. *Macromolecules.* 2004;37:3319–27.
26. Hu Z, Huang H, Zhang F, Du B, He T. Thickness-dependent molecular chain and lamellar crystal orientation in ultrathin poly(di-n-hexylsilane) films. *Langmuir.* 2004;20:3271–7.
27. Rueda DR, Hernández JJ, García-Gutiérrez MC, Ezquerro TA, Soccio M, Lotti N, et al. Flat-on lamellae in spin-coated, stable films of poly(propylene azelate). *Langmuir.* 2010;26:17540–5.
28. Maillard D, Prud'homme RE. Crystallization of ultrathin films of polylactides: from chain chirality to lamella curvature and twisting. *Macromolecules.* 2008;41:1705–12.
29. Wang Y, Chan C-M, Ng K-M, Li L. What controls the lamellar orientation at the surface of polymer films during crystallization? *Macromolecules.* 2008;41:2548–53.
30. Sun X, Guo L, Sato H, Ozaki Y, Yan S, Takahashi I. A study on the crystallization behavior of poly( $\beta$ -hydroxybutyrate) thin films on Si wafers. *Polymer.* 2011;52:3865–70.
31. Yang J-P, Liao Q, Zhou J-J, Jiang X, Wang X-H, Zhang Y, et al. What determines the lamellar orientation on substrates? *Macromolecules.* 2011;44:3511–6.
32. Zhou J-J, Liu J-G, Yan S-K, Dong J-Y, Li L, Chan C-M, et al. Atomic force microscopy study of the lamellar growth of isotactic polypropylene. *Polymer.* 2005;46:4077–87.
33. Wang X, Hou W, Zhou J, Li L, Li Y, Chan C-M. Melting behavior of lamellae of isotactic polypropylene studied using hot-stage atomic force microscopy. *Colloid Polym Sci.* 2007;285:449–55.
34. Padden FJ, Keith HD. Crystallization in thin films of isotactic polypropylene. *J Appl Phys.* 1966;37:4013–20.
35. Zhang B, Chen J, Liu B, Wang B, Shen C, Reiter R, et al. Morphological changes of isotactic polypropylene crystals grown in thin films. *Macromolecules.* 2017;50:6210–7.
36. Koga T, Morita M, Ishida H, Yakabe H, Sasaki S, Sakata O, et al. Dependence of the molecular aggregation state of octadecylsiloxane monolayers on preparation methods. *Langmuir.* 2005;21:905–10.
37. Owens DK, Wendt R. Estimation of the surface free energy of polymers. *J Appl Polym Sci.* 1969;13:1741–7.
38. Masunaga H, Ogawa H, Takano T, Sasaki S, Goto S, Tanaka T, et al. Multipurpose soft-material SAXS/WAXS/GISAXS beamline at SPring-8. *Polym J.* 2011;43:471–7.
39. Ogawa H, Masunaga H, Sasaki S, Goto S, Tanaka T, Seike T, et al. Experimental station for multiscale surface structural analyses of soft-material films at SPring-8 via a GISWAX/GIXD/XR-integrated system. *Polym J.* 2013;45:109–16.
40. Hatsui T, Graafsma H. X-ray imaging detectors for synchrotron and XFEL sources. *IUCrJ.* 2015;2:371–83.
41. Giannuzzi LA, Stevie FA. A review of focused ion beam milling techniques for TEM specimen preparation. *Micron.* 1999;30:197–204.
42. Norton DR, Keller A. The spherulitic and lamellar morphology of melt-crystallized isotactic polypropylene. *Polymer.* 1985;26:704–16.
43. Yamada K, Kajioaka H, Nozaki K, Toda A. Morphology and growth of single crystals of isotactic polypropylene from the melt. *J Macromol Sci Part B Phys.* 2010;50:236–47.
44. Clark EJ, Hoffman JD. Regime III crystallization in polypropylene. *Macromolecules.* 1984;17:878–85.
45. Roe R-J. Surface tension of polymer liquids. *J Phys Chem.* 1968;72:2013–7.
46. Theodorou DN. Variable-density model of polymer melt surfaces: structure and surface tension. *Macromolecules.* 1989;22:4578–89.
47. Beers KL, Douglas JF, Amis EJ, Karim A. Combinatorial measurements of crystallization growth rate and morphology in thin films of isotactic polystyrene. *Langmuir.* 2003;19:3935–40.
48. Binsbergen FL, de Lange BGM. Morphology of polypropylene crystallized from the melt. *Polymer.* 1968;9:23–40.